



# HOKKAIDO UNIVERSITY

Title	Modification of triaxial deformation and change of spectrum in $\Lambda$ 25Mg caused by the $\Lambda$ hyperon
Author(s)	Isaka, Masahiro; Homma, Hiroaki; Kimura, Masaaki et al.
Citation	Physical Review C, 85(3), 034303 <a href="https://doi.org/10.1103/PhysRevC.85.034303">https://doi.org/10.1103/PhysRevC.85.034303</a>
Issue Date	2012-03
Doc URL	<a href="https://hdl.handle.net/2115/48726">https://hdl.handle.net/2115/48726</a>
Rights	©2012 American Physical Society
Type	journal article
File Information	PRC85-3_034303.pdf



**Modification of triaxial deformation and change of spectrum in  ${}_{\Lambda}^{25}\text{Mg}$  caused by the  $\Lambda$  hyperon**

Masahiro Isaka, Hiroaki Homma, and Masaaki Kimura

*Department of Physics, Hokkaido University, Sapporo 060-0810, Japan*

Akinobu Doté

*Institute of Particle and Nuclear Studies, KEK, Tsukuba, Ibaraki 305-0801, Japan*

Akira Ohnishi

*Yukawa Institute for Theoretical Physics, Kyoto University, Kyoto 606-8502, Japan*

(Received 9 August 2011; revised manuscript received 2 November 2011; published 6 March 2012)

The positive-parity states of  ${}_{\Lambda}^{25}\text{Mg}$  with a  $\Lambda$  hyperon in  $s$  orbit were studied with the antisymmetrized molecular dynamics for hypernuclei. We discuss two bands of  ${}_{\Lambda}^{25}\text{Mg}$  corresponding to the  $K^{\pi} = 0^{+}$  and  $2^{+}$  bands of  ${}^{24}\text{Mg}$ . It is found that the energy of the  $K^{\pi} = 2^{+} \otimes \Lambda_s$  band is shifted up by about 200 keV compared to  ${}^{24}\text{Mg}$ . This is because the  $\Lambda$  hyperon in  $s$  orbit reduces the quadrupole deformation of the  $K^{\pi} = 0^{+} \otimes \Lambda_s$  band, while it does not change the deformation of the  $K^{\pi} = 2^{+} \otimes \Lambda_s$  band significantly.

DOI: [10.1103/PhysRevC.85.034303](https://doi.org/10.1103/PhysRevC.85.034303)

PACS number(s): 21.80.+a, 21.10.Pc, 21.60.Ka, 27.30.+t

**I. INTRODUCTION**

In recent decades, our knowledge of  $\Lambda$  hypernuclear spectra and the  $\Lambda N$  interaction has been greatly increased. Development of hypernuclear gamma-ray spectroscopy has enabled us to obtain precise excitation energies [1–3]. By analyzing these hypernuclear spectra theoretically and experimentally, most of the central part of the  $\Lambda N$  effective interaction has been clarified [3–10]. As a consequence, this makes it possible to investigate the structure of various  $\Lambda$  hypernuclei systematically and quantitatively.

By using such effective  $\Lambda N$  interactions, many theoretical studies predicted and revealed unique hypernuclear phenomena caused by the  $\Lambda$  hyperon. For example, changes of deformation, the supersymmetric state (or genuine hypernuclear state), and shrinkage of the intercluster distance were discussed in  $p$ -shell hypernuclei [6,11–20], and some of them are confirmed by experiments [2,3,21,22]. Recently, various structure changes have been predicted in  $sd$ -shell hypernuclei, because normal  $sd$ -shell nuclei have a variety of structures in the ground and low-lying states. For example, it was predicted that the  $\Lambda$  hyperon in  $s$  orbit reduces the nuclear deformation [17–20,23]. On the contrary, the  $\Lambda$  hyperon in  $p$  orbit enhances it [20]. In  ${}_{\Lambda}^{21}\text{Ne}$ , it was predicted that the  $\Lambda$  hyperon generates various  $\alpha + {}^{16}\text{O} + \Lambda$  cluster states [24]. By adding a  $\Lambda$  particle to the  $K^{\pi} = 2^{-}$  band, the mean-field-like states are also generated [25]. The difference between these structures leads to the difference in the  $\Lambda$  binding energies and the reduction of the  $B(E2)$  [25].

Up to now, many studies have been focused on the structure change of the hypernuclei with axial deformation and/or axial symmetric cluster structure such as  ${}_{\Lambda}^9\text{Be}$  and  ${}_{\Lambda}^{21}\text{Ne}$ . Although many nuclei are considered to have axially symmetric deformation, the degree of freedom of triaxial deformation plays an important role in nuclei with shape coexistence, and in nuclei soft against  $\gamma$  deformation [26–32].

In triaxial deformed nuclei, the response to the addition of the  $\Lambda$  particle will be different from those of axial symmetric nuclei [23,33,34].  ${}^{24}\text{Mg}$  is one of the candidates of triaxial deformed nuclei, because of the presence of the  $K^{\pi} = 2^{+}$  sideband built on the  $2_2^{+}$  state at 4.3 MeV [35–40]. Based on Skyrme-Hartree-Fock + BCS studies, it was predicted that the addition of a  $\Lambda$  particle makes  ${}_{\Lambda}^{25}\text{Mg}$  slightly soft against  $\gamma$  deformation [33]. And, a  $\Lambda$  particle slightly stretches the ground band and reduces the  $B(E2; 2_1^{+} \rightarrow 0^{+})$  [34]. However, in these studies, the quadrupole collective motion of  ${}_{\Lambda}^{25}\text{Mg}$  is treated in an approximated way by mapping the energy surface to the collective Hamiltonian. For quantitative discussions, more sophisticated treatment of deformation is desirable. Furthermore, the properties of the  $K^{\pi} = 2^{+}$  band are essential for the discussion of  $\gamma$  deformation, since it is quite sensitive to the  $\gamma$  deformation.

The aim of the present study is to reveal how the  $\Lambda$  hyperon affects triaxial deformation and the observables such as excitation energy and  $B(E2)$ . To investigate them quantitatively, three-dimensional angular momentum projection and the generator coordinate method (GCM) are known to be very powerful and indispensable. Therefore we have applied the HyperAMD with the GCM (HyperAMD + GCM) to  ${}_{\Lambda}^{25}\text{Mg}$ . The HyperAMD [25] is an extended version of the AMD (antisymmetrized molecular dynamics) for hypernuclei and describes hypernuclei without any assumption on the symmetry of nuclei. Combined with the GCM method, it is possible to investigate and predict the low-lying energy spectra and  $B(E2)$ , quantitatively.

In this study, we focus on two positive-parity bands of  ${}_{\Lambda}^{25}\text{Mg}$  with a  $\Lambda$  hyperon in  $s$  orbit corresponding to the  $K^{\pi} = 0^{+}$  (ground) and  $K^{\pi} = 2^{+}$  bands of  ${}^{24}\text{Mg}$ , and we call the former  $K^{\pi} = 0^{+} \otimes \Lambda_s$  and the latter  $K^{\pi} = 2^{+} \otimes \Lambda_s$ . It is found that the excitation energy of the  $K^{\pi} = 2^{+} \otimes \Lambda_s$  band is shifted up by about 200 keV systematically. This is due to the difference in the binding energy of the  $\Lambda$  hyperon,  $b_{\Lambda}$ , between the  $K^{\pi} = 0^{+} \otimes \Lambda_s$  and  $K^{\pi} = 2^{+} \otimes \Lambda_s$  bands.

This difference of  $b_\Lambda$  originates in the reduction of the nuclear quadrupole deformation in the  $K^\pi = 0^+ \otimes \Lambda_s$  band, while the  $\Lambda$  hyperon does not change that in the  $K^\pi = 2^+ \otimes \Lambda_s$  band significantly. However, the level spacing within each band is not changed by the  $\Lambda$  hyperon.

This paper is organized as follows. In the next section, we explain the theoretical framework of HyperAMD + GCM. In Sec. III, the low-lying states with positive parity of  ${}^{25}_\Lambda\text{Mg}$  and their properties are discussed. The differences between the  $K^\pi = 0^+ \otimes \Lambda_s$  and  $K^\pi = 2^+ \otimes \Lambda_s$  bands are the focus. The final section summarizes this work.

## II. FRAMEWORK

In this study, we applied the HyperAMD [25], which is an extended version of AMD for the hypernucleus, to  ${}^{25}_\Lambda\text{Mg}$ . To analyze low-lying spectra, the generator coordinate method (GCM) was also employed.

### A. Hamiltonian and variational wave function

The Hamiltonian used in this study is given as

$$\hat{H} = \hat{H}_N + \hat{H}_\Lambda - \hat{T}_g, \quad (1)$$

$$\hat{H}_N = \hat{T}_N + \hat{V}_{NN} + \hat{V}_{\text{Coul}}, \quad (2)$$

$$\hat{H}_\Lambda = \hat{T}_\Lambda + \hat{V}_{\Lambda N}. \quad (3)$$

Here  $\hat{T}_N$ ,  $\hat{T}_\Lambda$ , and  $\hat{T}_g$  are the kinetic energies of nucleons, a  $\Lambda$  hyperon, and the center-of-mass motion, respectively. We have used the Gogny D1S interaction [41] as an effective nucleon-nucleon interaction  $\hat{V}_{NN}$ . The Coulomb interaction  $\hat{V}_{\text{Coul}}$  is approximated by the sum of seven Gaussians. To see the dependence on the  $\Lambda N$  interaction, a couple of  $\Lambda N$  effective interactions  $\hat{V}_{\Lambda N}$  are examined. We have used  $YN$   $G$ -matrix interactions YNG-NF, YNG-ND, and YNG-NS [5]. The YNG interactions depend on the nuclear Fermi momentum  $k_F$  through the density dependence of the  $G$  matrix in the nuclear medium. In this work, we apply  $k_F = 1.18 \text{ fm}^{-1}$ . This gives the binding energy of the  $\Lambda$  particle in  ${}^{25}_\Lambda\text{Mg}$ ,  $B_\Lambda = 15.98 \text{ MeV}$  for YNG-NF,  $18.46 \text{ MeV}$  for YNG-ND, and  $15.18 \text{ MeV}$  for YNG-NS, and these values are consistent with the systematics of  $B_\Lambda$  as a function of mass number  $A$  derived from observed data [42].

The single  $\Lambda$  hypernucleus composed of  $A$  nucleons and a  $\Lambda$  hyperon is described by the wave function that is an eigenstate of the parity,

$$\Psi^\pi = \hat{P}^\pi \Psi_{\text{int}}, \quad (4)$$

where  $\hat{P}^\pi$  is the parity projector and the intrinsic wave function  $\Psi_{\text{int}}$  is represented by the direct product of the  $\Lambda$  single-particle wave function  $\varphi_\Lambda$  and the wave function of  ${}^{24}\text{Mg}$ ,  $\Psi_N$ ,

$$\Psi_{\text{int}} = \varphi_\Lambda \otimes \Psi_N. \quad (5)$$

The nuclear part is described by a Slater determinant of nucleon single-particle wave packets,

$$\Psi_N = \frac{1}{\sqrt{A!}} \det\{\psi_i(r_j)\}, \quad (6)$$

$$\psi_i(r_j) = \phi_i(r_j) \chi_i \eta_i, \quad (7)$$

$$\phi_i(r) = \prod_{\sigma=x,y,z} \left( \frac{2\nu_\sigma}{\pi} \right)^{1/4} \exp\left\{ -\nu_\sigma (r - Z_i)_\sigma^2 \right\}, \quad (8)$$

$$\chi_i = \alpha_i \chi_\uparrow + \beta_i \chi_\downarrow, \quad (9)$$

$$\eta_i = \text{proton or neutron}, \quad (10)$$

where  $\psi_i$  is the  $i$ th-nucleon single-particle wave packet consisting of spatial  $\phi_i$ , spin  $\chi_i$ , and isospin  $\eta_i$  parts. The centroids of Gaussian  $Z_i$ , width parameters  $\nu_\sigma$ , and spin directions  $\alpha_i$  and  $\beta_i$  are the variational parameters of the nuclear part.

The  $\Lambda$  single-particle wave function is represented by the superposition of Gaussian wave packets,

$$\varphi_\Lambda(r) = \sum_{m=1}^M c_m \varphi_m(r), \quad \varphi_m(r) = \phi_m(r) \chi_m, \quad (11)$$

$$\phi_m(r) = \prod_{\sigma=x,y,z} \left( \frac{2\nu_\sigma \mu}{\pi} \right)^{1/4} \exp\left\{ -\nu_\sigma \mu (r - z_m)_\sigma^2 \right\}, \quad (12)$$

$$\chi_m = a_m \chi_\uparrow + b_m \chi_\downarrow, \quad (13)$$

$$\mu = \frac{m_\Lambda}{m_N}, \quad (14)$$

where  $m_\Lambda$  and  $m_N$  represent the masses of the  $\Lambda$  particle and the nucleon, respectively. Again, the centroid of Gaussian  $z_m$ , spin directions  $a_m$  and  $b_m$ , and coefficients  $c_m$  are the variational parameters of the hyperon part. Since we have superposed Gaussian wave packets, it is rather tedious to remove the spurious center-of-mass kinetic energy exactly. Therefore we approximately removed it in the same way as our previous work [25].

### B. Variation on $\beta$ - $\gamma$ plane

The variational calculation has been performed in two steps. The first is the variational calculation for  ${}^{24}\text{Mg}$  under the constraints on nuclear matter quadrupole deformation parameters  $\beta$  and  $\gamma$ . The  $\beta$ - $\gamma$  constraint is applied in the same way as in Refs. [40,43]. The variation with the  $\beta$ - $\gamma$  constraint was achieved by addition of the parabolic potentials,

$$V_c = v_\beta (\langle \beta \rangle - \beta_i)^2 + v_\gamma (\langle \gamma \rangle - \gamma_i)^2, \quad (15)$$

$$\tilde{E} = \frac{\langle \Psi_N^\pi | \hat{H} | \Psi_N^\pi \rangle}{\langle \Psi_N^\pi | \Psi_N^\pi \rangle} + V_c, \quad (16)$$

to the total energy of the core nucleus  ${}^{24}\text{Mg}$ . The variational wave function of the nucleon part was determined to minimize  $\tilde{E}$  for given values of  $\beta_i$  and  $\gamma_i$  by using the frictional cooling method. The resulting nuclear wave function  $\Psi_N^\pi(\beta_i, \gamma_i)$  has minimum energy for a given set of  $(\beta_i, \gamma_i)$  and we shall call it the core state. In this study, the core states are calculated for discrete sets of  $(\beta_i, \gamma_i)$  in the  $\beta$ - $\gamma$  plane.

The second step is the variation for  ${}^{25}_\Lambda\text{Mg}$ . Combined with the core-state wave function  $\Psi_N^\pi(\beta_i, \gamma_i)$  as  $\Psi^\pi(\beta_i, \gamma_i) = \varphi_\Lambda \otimes \Psi_N^\pi(\beta_i, \gamma_i)$ , we have performed variational calculation of the  $\Lambda$  single-particle wave function and determined the variational parameters  $z_m$ ,  $a_m$ ,  $b_m$ , and  $c_m$  for each grid point on the

$\beta$ - $\gamma$  plane. We shall call the resulting state  $\Psi^\pi(\beta_i, \gamma_i)$  the hypernuclear state.

### C. Angular momentum projection and GCM

After the variational calculation, we project out an eigenstate of the total angular momentum from the hypernuclear states,

$$\Psi_{MK}^{J\pi}(\beta_i, \gamma_i) = \hat{P}_{MK}^J \Psi^\pi(\beta_i, \gamma_i) / \sqrt{N_K^{J\pi}(\beta_i, \gamma_i)}, \quad (17)$$

$$\hat{P}_{MK}^J = \frac{2J+1}{8\pi^2} \int d\Omega D_{MK}^{*J}(\Omega) \hat{R}(\Omega), \quad (18)$$

$$N_K^{J\pi} = \langle \hat{P}_{MK}^J \Psi^\pi(\beta_i, \gamma_i) | \hat{P}_{MK}^J \Psi^\pi(\beta_i, \gamma_i) \rangle. \quad (19)$$

Here  $\hat{P}_{MK}^J$  is the total angular momentum projector. The integrals are performed numerically over three Euler angles  $\Omega$ .

We calculate the mixing between the different  $K$  states that have the same intrinsic deformation  $(\beta_i, \gamma_i)$ ,

$$\Psi_n^{J\pi}(\beta_i, \gamma_i) = \sum_{K=-J}^J f_{Kni} \Psi_{MK}^{J\pi}(\beta_i, \gamma_i), \quad (20)$$

and call it the  $K$ -mixed state. The coefficients  $f_{Kni}$  are determined through the double diagonalization of  $H_{KK'}$  and  $N_{KK'}$  defined as

$$H_{KK'} = \langle \Psi_{MK}^{J\pi}(\beta_i, \gamma_i) | \hat{H} | \Psi_{M'K'}^{J\pi}(\beta_i, \gamma_i) \rangle, \quad (21)$$

$$N_{KK'} = \langle \Psi_{MK}^{J\pi}(\beta_i, \gamma_i) | \Psi_{M'K'}^{J\pi}(\beta_i, \gamma_i) \rangle. \quad (22)$$

Finally, we superpose all of the  $K$ -mixed states with different deformations  $(\beta_i, \gamma_i)$  (GCM). Then the final wave function of the system becomes

$$\Psi_\alpha^{J\pi} = \sum_{i,n} g_{ni\alpha} \Psi_n^{J\pi}(\beta_i, \gamma_i), \quad (23)$$

where quantum numbers other than total angular momentum and parity are represented by  $\alpha$ . The coefficients  $g_{ni\alpha}$  are determined by the solving the Hill-Wheeler equation:

$$\sum_{n',j} H_{nin'j} g_{n'j\alpha} = E_\alpha \sum_{n',j} N_{nin'j} g_{n'j\alpha}, \quad (24)$$

$$H_{nin'j} = \langle \Psi_n^{J\pi}(\beta_i, \gamma_i) | \hat{H} | \Psi_{n'}^{J\pi}(\beta_j, \gamma_j) \rangle, \quad (25)$$

$$N_{nin'j} = \langle \Psi_n^{J\pi}(\beta_i, \gamma_i) | \Psi_{n'}^{J\pi}(\beta_j, \gamma_j) \rangle. \quad (26)$$

The physical quantities discussed in the next section are basically calculated from the GCM wave function.

### D. Analysis of wave function

To analyze and discuss the GCM wave function on the  $\beta$ - $\gamma$  plane, it is convenient to introduce the overlap between the GCM wave function  $\Psi_n^{J\pi}$  and  $K$ -mixed states,

$$O_{n\alpha}^{J\pi}(\beta_i, \gamma_i) = | \langle \Psi_n^{J\pi}(\beta_i, \gamma_i) | \Psi_\alpha^{J\pi} \rangle |^2. \quad (27)$$

The behavior of  $O_{n\alpha}^{J\pi}(\beta_i, \gamma_i)$  in the  $\beta$ - $\gamma$  plane is discussed in the next section.

We also calculate the expectation values of the operators  $\hat{H}_\Lambda$  and  $\hat{H}_N$ ,

$$b_\Lambda = -\langle \Psi_\alpha^{J\pi} | \hat{H}_\Lambda | \Psi_\alpha^{J\pi} \rangle, \quad (28)$$

$$E_N = \langle \Psi_\alpha^{J\pi} | \hat{H}_N | \Psi_\alpha^{J\pi} \rangle, \quad (29)$$

to see the contribution from the hyperon part and nuclear part to energy shifts. For further analysis, by using the  $K$ -mixed state Eq. (20) with given deformation parameters  $\beta_i$  and  $\gamma_i$ , we calculate the expectation values of the operators  $\hat{H}$  and  $\hat{H}_\Lambda$ ,

$$\epsilon(\beta_i, \gamma_i) = \langle \Psi_n^{J\pi}(\beta_i, \gamma_i) | \hat{H} | \Psi_n^{J\pi}(\beta_i, \gamma_i) \rangle, \quad (30)$$

$$b'_\Lambda(\beta_i, \gamma_i) = -\langle \Psi_n^{J\pi}(\beta_i, \gamma_i) | \hat{H}_\Lambda | \Psi_n^{J\pi}(\beta_i, \gamma_i) \rangle. \quad (31)$$

## III. RESULTS AND DISCUSSION

The calculated and observed energy spectra of  $^{24}\text{Mg}$  are presented in Fig. 1. In  $^{24}\text{Mg}$ , we have performed the GCM calculation by using basis wave functions with axial and triaxial deformation. To investigate the effect of the  $\gamma$  deformation, we have also performed the symmetry-restricted GCM calculation, in which the basis wave functions are limited to axial symmetric states ( $\gamma = 0^\circ$  or  $60^\circ$ ). We call the former triaxial GCM and the latter axial GCM. The axial GCM and triaxial GCM results are shown in Fig. 1(b) and Fig. 1(c), respectively. Figure 1(c) shows that the triaxial GCM result describes successfully the ground ( $K^\pi = 0^+$ ) and the  $K^\pi = 2^+$  bands. The dotted line at 9.32 MeV represents the experimental  $\alpha + ^{20}\text{Ne}$  threshold energy corresponding to the lowest decay channel. In  $^{24}\text{Mg}$ , a triaxial deformation of low-lying states has been discussed by many authors [35–40]. The excitation energy of the  $K^\pi = 2^+$  band is quite sensitive to the degree of freedom of triaxial deformation. If triaxial deformation is not included, the theoretical calculations overestimate the excitation energy of the  $2_2^+$  state by about 4 MeV [38,40]. Indeed, Fig. 1(b) shows that the axial GCM calculation fails to reproduce the excitation energy of the  $K^\pi = 2^+$  band, while it reproduces the  $K^\pi = 0^+$  band as the results of the triaxial GCM. This indicates that the excitation energy of the  $K^\pi = 2^+$  band becomes higher, as its deformation is changed to the axial symmetric deformation. On the other hand, the excitation energy of the  $K^\pi = 0^+$  band is almost unchanged, though its deformation is changed from the triaxial to axial deformation. Figures 2(a)–2(c) display the density distributions of the intrinsic wave functions which contribute largely to the  $0_1^+$  and  $2_2^+$  states of  $^{24}\text{Mg}$ . It confirms triaxial deformation of  $^{24}\text{Mg}$ .

### A. Energy spectra of $^{25}_\Lambda\text{Mg}$

Figure 1(d) shows the low-lying spectrum of  $^{25}_\Lambda\text{Mg}$  obtained by using the YNG-NF interaction. We focus on two bands corresponding to the  $K^\pi = 0^+$  and  $K^\pi = 2^+$  bands of  $^{24}\text{Mg}$  generated by adding a  $\Lambda$  hyperon in  $s$  orbit. We call the former the  $K^\pi = 0^+ \otimes \Lambda_s$  band, and the latter the  $K^\pi = 2^+ \otimes \Lambda_s$  band. Coupling of a  $\Lambda$  hyperon in  $s$  orbit to the nonzero  $J$  states generates the doublets with  $J - 1/2$  and  $J + 1/2$ . However, most of them are degenerated in Fig. 1. The dotted line in

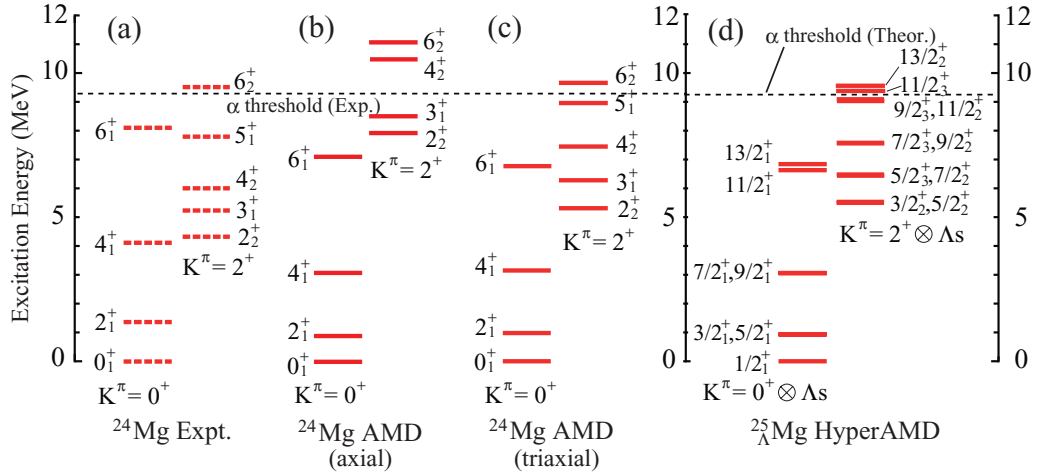


FIG. 1. (Color online) (a) Observed low-lying energy spectra of  $^{24}\text{Mg}$ . (b), (c) Calculated energy spectra of axial GCM and triaxial GCM, respectively. (d) Corresponding spectra of  $^{25}_{\Lambda}\text{Mg}$  with  $\Lambda$  hyperon in  $s$  orbit.

Fig. 1(d) represents the  $\alpha + ^{21}_{\Lambda}\text{Ne}$  threshold energy calculated with HyperAMD. It shows that both the  $K^{\pi} = 0^{+} \otimes \Lambda_s$  and  $K^{\pi} = 2^{+} \otimes \Lambda_s$  bands will bound.

Figures 2(d)–2(e) display the intrinsic density distribution for the  $3/2^{+}$  state of  $^{25}_{\Lambda}\text{Mg}$  belonging to the  $K^{\pi} = 2^{+} \otimes \Lambda_s$  band. It shows that the nuclear density distribution of the  $3/2^{+}$  state in  $^{25}_{\Lambda}\text{Mg}$  has triaxial deformation. Therefore, the contribution from the intrinsic state with triaxial deformation is important in  $^{25}_{\Lambda}\text{Mg}$  as in the case of  $^{24}\text{Mg}$ . The distribution of the  $\Lambda$  hyperon is also triaxially deformed. Therefore the  $\Lambda$  hyperon orbit is not pure  $s$  orbit but nonzero angular momentum components are also mixed. In this paper, we call it  $s$  orbit approximately.

Although the drastic changes cannot be seen in Fig. 1, the  $\Lambda$  hyperon changes the excitation energies quantitatively. In Table I, the excitation energies of each state in  $^{24}\text{Mg}$  and  $^{25}_{\Lambda}\text{Mg}$  are listed. It shows that the excitation energy of the  $K^{\pi} = 2^{+} \otimes \Lambda_s$

$\Lambda_s$  band is shifted up by about  $\Delta E_x = 200$  keV systematically. On the other hand, the level spacing within the  $K^{\pi} = 0^{+} \otimes \Lambda_s$  and  $K^{\pi} = 2^{+} \otimes \Lambda_s$  bands hardly change by a  $\Lambda$  hyperon. This trend of the level spacing in the  $K^{\pi} = 0^{+} \otimes \Lambda_s$  band is different from the prediction in Ref. [34], where the authors predicted that the  $\Lambda$  hyperon slightly stretches the spectra of the ground band, due to the reduction of the  $\beta$  deformation. It is found that the band head of the  $K^{\pi} = 2^{+}$  band is shifted up by using the YNG-ND and YNG-NS interactions by 290 keV

TABLE I. Excitation energies (MeV) of each state in the  $K^{\pi} = 0^{+}$  and  $K^{\pi} = 2^{+}$  bands of  $^{24}\text{Mg}$  and the corresponding states of  $^{25}_{\Lambda}\text{Mg}$ . Changes of excited energies  $\Delta E_x$  for each state obtained with AMD are also presented in units of MeV. For comparison, observed energies are also listed [44].

$^{24}\text{Mg}$			$^{25}_{\Lambda}\text{Mg}$		
$K^{\pi} = 0^{+}$	$E_x$ (Cal.)	$E_x$ (Exp.)	$0^{+} \otimes \Lambda_s$	$E_x$ (Cal.)	$\Delta E_x$
$0_1^{+}$	0.00	0.00	$1/2_1^{+}$	0.00	$\pm 0.00$
$2_1^{+}$	0.98	1.37	$3/2_1^{+}$	0.94	$-0.04$
			$5/2_1^{+}$	0.93	$-0.05$
$4_1^{+}$	3.15	4.12	$7/2_1^{+}$	3.06	$-0.09$
			$9/2_1^{+}$	3.06	$-0.09$
$6_1^{+}$	6.77	8.11	$11/2_1^{+}$	6.63	$-0.14$
			$13/2_1^{+}$	6.84	$+0.07$
$^{24}\text{Mg}$			$^{25}_{\Lambda}\text{Mg}$		
$K^{\pi} = 2^{+}$	$E_x$ (Cal.)	$E_x$ (Exp.)	$2^{+} \otimes \Lambda_s$	$E_x$ (Cal.)	$\Delta E_x$
$2_2^{+}$	5.31	4.33	$3/2_2^{+}$	5.53	$+0.22$
			$5/2_2^{+}$	5.50	$+0.19$
$3_1^{+}$	6.28	5.24	$5/2_3^{+}$	6.44	$+0.16$
			$7/2_2^{+}$	6.48	$+0.20$
$4_2^{+}$	7.45	6.01	$7/2_3^{+}$	7.56	$+0.11$
			$9/2_2^{+}$	7.58	$+0.13$
$5_1^{+}$	8.96	7.81	$9/2_3^{+}$	9.03	$+0.07$
			$11/2_2^{+}$	9.09	$+0.13$
$6_2^{+}$	9.66	9.53	$11/2_3^{+}$	9.38	$-0.22$
			$13/2_2^{+}$	9.56	$-0.10$

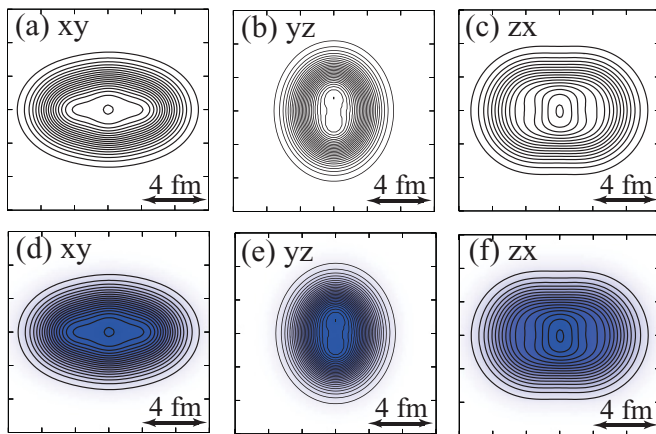


FIG. 2. (Color online) Density distributions of the intrinsic wave functions that contribute largely to the  $2_1^{+}$  and  $2_2^{+}$  states of  $^{24}\text{Mg}$  (upper panels) and to the  $3/2_1^{+}$  and  $3/2_2^{+}$  states of  $^{25}_{\Lambda}\text{Mg}$  (bottom panels) plotted from different directions, respectively. Solid lines show the nuclear density distributions, while the color plots represent the distributions of the  $\Lambda$  hyperon.

TABLE II. Total energy  $E$ , changes of  $E_N$ ,  $\Delta E_N$ , and  $b_\Lambda$  are listed in units of MeV. Definition of  $\Delta E_N$  is given in text.

States	$K^\pi = 0^+ \otimes \Lambda_s$ band		$b_\Lambda$
	$E$	$\Delta E_N$	
$1/2_1^+$	-213.83	+0.08	15.98
$3/2_1^+$	-212.89	+0.04	15.99
$5/2_1^+$	-212.89	+0.04	15.99
$7/2_1^+$	-210.77	+0.02	16.03
$9/2_1^+$	-210.76	+0.04	16.04
States	$K^\pi = 2^+ \otimes \Lambda_s$ band		$b_\Lambda$
	$E$	$\Delta E_N$	
$3/2_2^+$	-208.30	+0.10	15.80
$5/2_2^+$	-208.33	+0.07	15.79
$5/2_3^+$	-207.39	+0.03	15.79
$7/2_2^+$	-207.35	+0.07	15.79
$7/2_3^+$	-206.27	+0.01	15.82
$9/2_2^+$	-206.25	+0.04	15.82

and 210 keV, respectively. Since the YNG-ND and YNG-NS interactions give the qualitatively same results as the YNG-NF interaction, we focus on the YNG-NF result in the following.

### B. Difference in $b_\Lambda$ between the $K^\pi = 0^+ \otimes \Lambda_s$ and $K^\pi = 2^+ \otimes \Lambda_s$ bands

The increase of the excitation energy of the  $K^\pi = 2^+ \otimes \Lambda_s$  band is due to the difference in the  $\Lambda$  binding energy  $b_\Lambda$  between the  $K^\pi = 0^+ \otimes \Lambda_s$  and  $K^\pi = 2^+ \otimes \Lambda_s$  bands. Table II summarizes the  $b_\Lambda$  defined by Eq. (28) for each hypernuclear state in the  $K^\pi = 0^+ \otimes \Lambda_s$  and  $K^\pi = 2^+ \otimes \Lambda_s$  bands. For comparison, we calculated the energy changes of the nuclear part,  $\Delta E_N$ , as

$$\Delta E_N = E_N(^{25}\text{Mg}(J^\pi)) - E(^{24}\text{Mg}(j^\pi)), \quad (32)$$

where  $E_N$  is defined by Eq. (29). The total energy  $E$  and  $\Delta E_N$  obtained after the GCM calculation are also listed in Table II. It shows that the  $b_\Lambda$  for the  $K^\pi = 0^+ \otimes \Lambda_s$  band is larger than that for the  $K^\pi = 2^+ \otimes \Lambda_s$  band by 200 keV systematically. On the other hand, the effects of the  $\Lambda$  particle on the nuclear part are small and comparable for the  $K^\pi = 0^+$  and  $K^\pi = 2^+$  bands. Combining Eqs. (28), (29), and (32), one finds the relation

$$\Delta E_x = E_x(^{25}\text{Mg}(J^\pi)) - E_x(^{24}\text{Mg}(j^\pi)) \quad (33)$$

$$= \Delta E_N - b_\Lambda + B_\Lambda, \quad (34)$$

$$B_\Lambda = E(^{24}\text{Mg}(GS)) - E(^{25}\text{Mg}(GS)), \quad (35)$$

where  $\Delta E_x$  is change of excitation energy between  $^{24}\text{Mg}$  and  $^{25}\text{Mg}$  for each state and we have obtained the  $B_\Lambda = 15.91$  MeV. Therefore the difference of the  $\Delta E_x$  between the  $K^\pi = 0^+ \otimes \Lambda_s$  and  $K^\pi = 2^+ \otimes \Lambda_s$  bands comes from the difference of  $b_\Lambda$  between these bands.

The difference of  $b_\Lambda$  between the  $K^\pi = 0^+ \otimes \Lambda_s$  and  $K^\pi = 2^+ \otimes \Lambda_s$  bands comes from the difference of the deformation change by  $\Lambda$  hyperon between these bands.

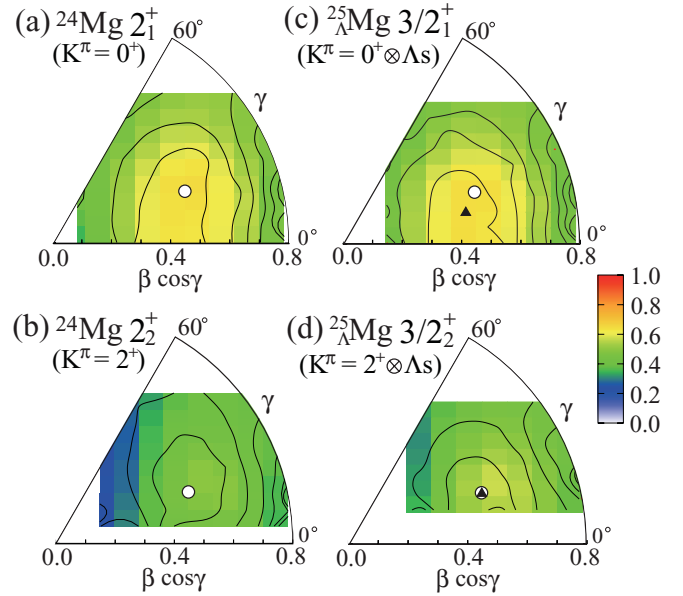


FIG. 3. (Color online) Contour line represents the increase of  $\epsilon(\beta, \gamma)$  for every 1 MeV, and color plots show the distribution of the GCM overlap. The definition of  $\epsilon(\beta, \gamma)$  and the GCM overlap are given by Eq. (30) and Eq. (27), respectively. (a) and (b) correspond to the  $2_1^+$  states of the  $K^\pi = 0^+$  band and the  $2_2^+$  state of the  $K^\pi = 2^+$  band of  $^{24}\text{Mg}$ , respectively. Open circles represent the peak positions of the GCM overlap for the  $2_1^+$  and  $2_2^+$  states, respectively. (c) and (d) correspond to the  $3/2_1^+$  and  $3/2_2^+$  states of  $^{25}\text{Mg}$  with  $\Lambda$  hyperon in  $s$  orbit, respectively. Filled triangles show the peak positions of the GCM overlap for each state of  $^{25}\text{Mg}$ , while open circles show those of the GCM overlap for the corresponding states  $2_1^+$  and  $2_2^+$ , respectively.

The deformation change is clearly seen from the distribution of the GCM overlap defined by Eq. (27). In Fig. 3, the color plots display the distribution of the GCM overlap for the  $2_1^+$  and  $2_2^+$  states of  $^{24}\text{Mg}$  and for the  $3/2_1^+$  and  $3/2_2^+$  states of  $^{25}\text{Mg}$ . And the contour shows the increase of  $\epsilon(\beta, \gamma)$ , defined by Eq. (30). To obtain the  $\epsilon(\beta, \gamma)$ , we perform the diagonalization of  $K$  and obtain two eigenvalues for the  $J = 2$  state of  $^{24}\text{Mg}$  and the  $J = 3/2$  state of  $^{25}\text{Mg}$ , respectively. It is found that the lowest energy eigenstate corresponds to the  $2_1^+$  ( $3/2_1^+$ ) state of  $^{24}\text{Mg}$  ( $^{25}\text{Mg}$ ), and the second-lowest eigenstate corresponds to the  $2_2^+$  ( $3/2_2^+$ ) state of  $^{24}\text{Mg}$  ( $^{25}\text{Mg}$ ) at each  $(\beta_i, \gamma_i)$ .

In Fig. 3(a), the peak of the GCM overlap for the  $2_1^+$  state of  $^{24}\text{Mg}$  locates at  $(\beta, \gamma) = (0.48, 21^\circ)$ . Figure 3(b) shows that the peak of the GCM overlap also locates at  $(\beta, \gamma) = (0.48, 21^\circ)$  for the  $2_2^+$  state. In the case of the  $3/2_1^+$  state of the  $^{25}\text{Mg}$ , the peak position is shifted toward smaller  $\beta$  and  $\gamma$  compared to  $^{24}\text{Mg}$ , and located at  $(\beta, \gamma) = (0.43, 15^\circ)$ . On the contrary, in the case of the  $3/2_2^+$  state, the peak position is unchanged. Therefore the  $\Lambda$  hyperon in  $s$  orbit reduces the quadrupole deformation of the  $3/2_1^+$  state, while it does not change deformation of the  $3/2_2^+$  state.

Here we compare the  $b'_\Lambda(\beta, \gamma)$  of the  $3/2_1^+$  state with that of the  $3/2_2^+$  state in  $^{25}\text{Mg}$ . According to Eq. (31), we obtained  $b'_\Lambda(\beta = 0.43, \gamma = 15^\circ) = 16.09$  MeV for the  $3/2_1^+$  state, while  $b'_\Lambda(\beta = 0.48, \gamma = 21^\circ) = 15.80$  MeV for the

TABLE III. Deformation parameters  $\beta$  and  $\gamma$  corresponding to the peak of the GCM overlap are summarized.  $b'_\Lambda(\beta, \gamma)$  at the peak position of the GCM overlap for each state is also listed in units of MeV. Definition of  $b'_\Lambda(\beta, \gamma)$  is given by Eq. (31).

$^{24}\text{Mg}$			$^{25}_\Lambda\text{Mg}$			
$K^\pi = 0^+$	$\beta$	$\gamma$ (deg)	$0^+ \otimes \Lambda_s$	$\beta$	$\gamma$ (deg)	$b'_\Lambda$
$0^+_1$	0.48	21	$1/2^+_1$	0.48	21	15.90
$2^+_1$	0.48	21	$3/2^+_1$	0.43	15	16.09
			$5/2^+_1$	0.43	15	16.10
$4^+_1$	0.48	21	$7/2^+_1$	0.39	25	16.14
			$9/2^+_1$	0.39	25	16.15
$^{24}\text{Mg}$			$^{25}_\Lambda\text{Mg}$			
$K^\pi = 2^+$	$\beta$	$\gamma$ (deg)	$2^+ \otimes \Lambda_s$	$\beta$	$\gamma$ (deg)	$b'_\Lambda$
$2^+_2$	0.48	21	$3/2^+_2$	0.48	21	15.80
			$5/2^+_2$	0.48	21	15.80
$3^+_1$	0.48	21	$5/2^+_3$	0.48	21	15.79
			$7/2^+_2$	0.48	21	15.79
$4^+_2$	0.48	21	$7/2^+_3$	0.48	21	15.77
			$9/2^+_2$	0.48	21	15.78

$3/2^+_2$  state. Namely,  $b'_\Lambda(\beta, \gamma)$  of the  $3/2^+_1$  state is larger than that of the  $3/2^+_2$  state. This is because the nuclear quadrupole deformation of the  $3/2^+_1$  state is smaller than that of the  $3/2^+_2$  state. Therefore the  $\Lambda$  hyperon in  $s$  orbit gains the larger  $\Lambda$  binding energy for the  $3/2^+_1$  state.

The reason for the difference in the deformation change caused by the  $\Lambda$  hyperon is related to the dependence of the  $K^\pi = 0^+$  and  $K^\pi = 2^+$  bands of  $^{24}\text{Mg}$  on the triaxial deformation. Since the  $K^\pi = 0^+$  band of  $^{24}\text{Mg}$  does not depend on the triaxial deformation significantly, the nuclear deformation of  $^{25}_\Lambda\text{Mg}$  can be easily changed by adding the  $\Lambda$  hyperon. Therefore, the nuclear deformation of the  $3/2^+_1$  state becomes smaller so as to make the  $\Lambda$  binding energy larger. This is one of the shrinkage effects due to the  $\Lambda$  hyperon. On the other hand, the excitation energy of the  $K^\pi = 2^+$  band of  $^{24}\text{Mg}$  becomes higher, as its deformation is changed to axial deformation. This makes the nuclear part of  $^{25}_\Lambda\text{Mg}$  rigid against the shrinkage effect of the  $\Lambda$  hyperon. Therefore the nuclear deformation of the  $3/2^+_2$  state is unchanged despite the addition of the  $\Lambda$  hyperon.

This trend is common to the other excited states of  $^{25}_\Lambda\text{Mg}$ . Namely, the  $\Lambda$  hyperon changes the nuclear deformation in the  $K^\pi = 0^+ \otimes \Lambda_s$  band, while it does not affect the deformation in the  $K^\pi = 2^+ \otimes \Lambda_s$  band significantly. Table III presents the peak position of the GCM overlap and  $b'_\Lambda$  for each state of  $^{24}\text{Mg}$  and  $^{25}_\Lambda\text{Mg}$ . It shows that the peak position of the GCM overlap is shifted by adding the  $\Lambda$  hyperon in the  $K^\pi = 0^+ \otimes \Lambda_s$  band except for the  $1/2^+_1$  state. We found that the distribution of the GCM overlap in the  $1/2^+_1$  state is slightly shifted toward the smaller deformation. On the other hand, the peak position of the GCM overlap is unchanged in the  $K^\pi = 2^+ \otimes \Lambda_s$  band. In addition, the  $b'_\Lambda$  values of the  $K^\pi = 0^+ \otimes \Lambda_s$  band are larger than those of the  $K^\pi = 2^+ \otimes \Lambda_s$  band. This indicates that the nuclear deformation of the  $K^\pi = 0^+ \otimes \Lambda_s$  band is changed so as to make the  $\Lambda$  binding energy larger, while the deformation

TABLE IV. Intra- and interband  $B(E2)$  values ( $e^2 \text{fm}^4$ ) for the  $2^+_1 \rightarrow 0^+_1$  ( $K^\pi = 0^+$  band) and  $3^+_1 \rightarrow 2^+_2$  ( $K^\pi = 2^+$  band) transitions in  $^{24}\text{Mg}$  and the corresponding transitions in  $^{25}_\Lambda\text{Mg}$ .  $cB(E2)$  represents the corrected  $B(E2)$  values explained in the Appendix.

$^{24}\text{Mg}$ (AMD)		$^{25}_\Lambda\text{Mg}$ (HyperAMD)			
Transitions	$B(E2)$	Transitions	$B(E2)$	$cB(E2)$	Changes (%)
$2^+_1 \rightarrow 0^+_1$	98	$3/2^+_1 \rightarrow 1/2^+_1$	92	92	-6.1
		$5/2^+_1 \rightarrow 1/2^+_1$	92	92	-6.1
$3^+_1 \rightarrow 2^+_2$	167	$7/2^+_2 \rightarrow 3/2^+_2$	19	192	+15
		$7/2^+_2 \rightarrow 5/2^+_2$	160	178	+6.6
		$5/2^+_3 \rightarrow 3/2^+_2$	138	173	+3.4
		$5/2^+_3 \rightarrow 5/2^+_2$	39	195	+17

of the  $K^\pi = 2^+ \otimes \Lambda_s$  band is unchanged by adding the  $\Lambda$  hyperon. Therefore, the  $K^\pi = 2^+ \otimes \Lambda_s$  band is shifted up by about 200 keV.

In Table III, the  $\gamma$  deformation is somewhat enhanced in the  $7/2^+_1$  and  $9/2^+_1$  states, while it is reduced in the  $3/2^+_1$  and  $5/2^+_1$  states. This indicates that the change of the  $\gamma$  deformation can be different depending on the states. The reduction of the  $\beta$  deformation becomes large as angular momentum increases. Indeed, Table III shows that the  $\beta$  deformation of the  $7/2^+_1$  and  $9/2^+_1$  states is smaller than that of the  $3/2^+_1$  and  $5/2^+_1$  states. Since the  $4^+_1$  state of  $^{24}\text{Mg}$  prefers the large  $\gamma$  deformation at  $\beta \simeq 0.4$ , the  $\gamma$  deformation is slightly changed in the  $7/2^+_1$  and  $9/2^+_1$  states. The energy minima of the  $7/2^+_1$  and  $9/2^+_1$  states are shifted and locate at  $(\beta = 0.39, \gamma = 25^\circ)$ . Thus, the  $K^\pi = 0^+ \otimes \Lambda_s$  band is quite sensitive to the structure of the energy surface of each state in  $^{24}\text{Mg}$ .

### C. Changes of $B(E2)$ by $\Lambda$ hyperon

We have calculated the intra- and interband  $B(E2)$  values by using the GCM wave functions. To compare the  $B(E2)$  values of  $^{25}_\Lambda\text{Mg}$  with those of  $^{24}\text{Mg}$ , they are corrected under the assumption that a  $\Lambda$  hyperon occupies the  $s$  orbit for each hypernuclear state in the  $K^\pi = 0^+ \otimes \Lambda_s$  and  $K^\pi = 2^+ \otimes \Lambda_s$  bands (see the Appendix). Table IV summarizes both the uncorrected and corrected  $B(E2)$  values corresponding to the intra- and interband transitions  $2^+_1 \rightarrow 0^+_1$  in the  $K^\pi = 0^+$  band and  $3^+_1 \rightarrow 2^+_2$  in the  $K^\pi = 2^+$  band.

It is found that the  $\Lambda$  hyperon in  $s$  orbit does not change the  $B(E2)$  values significantly. Indeed, Table IV shows that the changes of  $B(E2)$  due to the  $\Lambda$  hyperon are less than 10% except for the  $7/2^+_2 \rightarrow 3/2^+_2$  and  $5/2^+_3 \rightarrow 5/2^+_2$  transitions, and are consistent with the prediction in Ref. [34]. These changes are smaller than the changes in  $^{21}_\Lambda\text{Ne}$ . In the case of  $^{21}_\Lambda\text{Ne}$ , it is predicted that the  $B(E2)$  values are reduced by about 20% by the calculation with the  $\alpha + ^{16}\text{O} + \Lambda$  cluster model [24] and HyperAMD + GCM [25]. We have calculated and investigated the change of  $B(E2)$  values for the interband transitions in  $^{25}_\Lambda\text{Mg}$ . It is found that the changes of  $B(E2)$  values of the intra- and interband transitions are also about 10%.

#### IV. SUMMARY

In this paper, we have applied the HyperAMD to  ${}^{25}_{\Lambda}\text{Mg}$  and investigated the effects by a  $\Lambda$  hyperon to the nucleus with triaxial deformation. Focusing on the positive-parity states with a  $\Lambda$  hyperon in  $s$  orbit, we discussed two bands of  ${}^{25}_{\Lambda}\text{Mg}$  corresponding to the  $K^{\pi} = 0^{+}$  and  $K^{\pi} = 2^{+}$  bands in  ${}^{24}\text{Mg}$ . Both of them are expected to be bound.

Although the gross feature of the excitation spectra of  ${}^{25}_{\Lambda}\text{Mg}$  remains similar to that of  ${}^{24}\text{Mg}$ , the  $\Lambda$  hyperon in  $s$  orbit changes the excitation energies quantitatively. It is found that the excitation energy of the  $K^{\pi} = 2^{+} \otimes \Lambda_s$  band in  ${}^{25}_{\Lambda}\text{Mg}$  is shifted up by 200 keV compared to that of the  $K^{\pi} = 2^{+}$  band in  ${}^{24}\text{Mg}$ . This comes from the difference of  $b_{\Lambda}$  between the  $K^{\pi} = 0^{+} \otimes \Lambda_s$  and  $K^{\pi} = 2^{+} \otimes \Lambda_s$  bands and it depends on the deformation change of these bands. Since the  $\Lambda$  hyperon reduces the nuclear quadrupole deformation of the  $K^{\pi} = 0^{+} \otimes \Lambda_s$  band, the  $\Lambda$  binding energy of the  $K^{\pi} = 0^{+} \otimes \Lambda_s$  is larger than that of the  $K^{\pi} = 2^{+} \otimes \Lambda_s$  band. On the other hand, the level spacing with the  $K^{\pi} = 0^{+} \otimes \Lambda_s$  and  $K^{\pi} = 2^{+} \otimes \Lambda_s$  bands does not change by adding a  $\Lambda$  hyperon significantly.

It is found that the changes of the intra- and interband  $B(E2)$  values are not large compared to the prediction of the  $B(E2)$  reduction for  ${}^{21}_{\Lambda}\text{Ne}$ . This corresponds to the small deformation changes by a  $\Lambda$  hyperon in  ${}^{25}_{\Lambda}\text{Mg}$ .

#### ACKNOWLEDGMENT

This work was supported by a Grant-in-Aid from the Japan Society for the Promotion of Science (No. 236937).

#### APPENDIX: CORRECTION OF $B(E2)$ VALUES

We assume the weak coupling limit in the same way as in Refs. [2,16], and compare the  $B(E2)$  values of  ${}^{25}_{\Lambda}\text{Mg}$  with the corresponding  $E2$  transitions of  ${}^{24}\text{Mg}$ . Here, we assume that the initial (final) state with angular momentum  $J_i$  ( $J_f$ ) of the  $\Lambda$  hypernucleus consists of a core state with angular momentum  $j_i^C$  ( $j_f^C$ ) and a  $\Lambda$  hyperon with  $j^{\Lambda} = 1/2$ . Thus,

$$|J_i M_i\rangle = \sum_{m_i^C, m_i^{\Lambda}} C_{m_i^C, m_i^{\Lambda}}^{J_i, M_i} |j_i^C m_i^C\rangle \otimes |j_i^{\Lambda} m_i^{\Lambda}\rangle,$$

$$|J_f M_f\rangle = \sum_{m_f^C, m_f^{\Lambda}} C_{m_f^C, m_f^{\Lambda}}^{J_f, M_f} |j_f^C m_f^C\rangle \otimes |j_f^{\Lambda} m_f^{\Lambda}\rangle,$$

where  $C_{m_1, m_2}^{j_3, m_3} = \langle j_3 m_3 | j_1 m_1, j_2 m_2 \rangle$  is a Clebsch-Gordan coefficient.

The corrected  $B(E2)$  value  $cB(E2)$  becomes

$$\begin{aligned} cB(E2, j_i^C \rightarrow j_f^C) &= \frac{2j_f^C + 1}{2j_i^C + 1} |\langle j_f^C || \hat{O}(E2) || j_i^C \rangle|^2 \\ &= \frac{2j_f^C + 1}{2j_i^C + 1} \frac{B(E2, J_i \rightarrow J_f)}{C}, \end{aligned}$$

where

$$C = \sum_{M_f} \left( \sum_{m_f^C, m_f^{\Lambda}} \sum_{m_i^C, m_i^{\Lambda}} C_{m_f^C, m_f^{\Lambda}}^{J_f, M_f} C_{m_i^C, m_i^{\Lambda}}^{J_i, M_i} C_{m_f^C, m_f^{\Lambda}}^{j_f^C, m_f^C} \right)^2,$$

$$m_i^{\Lambda} = m_f^{\Lambda} = m^{\Lambda}.$$

- 
- [1] H. Tamura, K. Tanida, D. Abe, H. Akikawa, K. Araki, H. Bhang, T. Endo, Y. Fujii, T. Fukuda, O. Hashimoto, K. Imai, H. Hotchi, Y. Kakiguchi, J. H. Kim, Y. D. Kim, T. Miyoshi, T. Murakami, T. Nagae, H. Noumi, H. Outa, K. Ozawa, T. Saito, J. Sasao, Y. Sato, S. Satoh, R. I. Sawafta, M. Sekimoto, T. Takahashi, L. Tang, H. H. Xia, S. H. Zhou, and L. H. Zhu, *Phys. Rev. Lett.* **84**, 5963 (2000).
- [2] K. Tanida, H. Tamura, D. Abe, H. Akikawa, K. Araki, H. Bhang, T. Endo, Y. Fujii, T. Fukuda, O. Hashimoto, K. Imai, H. Hotchi, Y. Kakiguchi, J. H. Kim, Y. D. Kim, T. Miyoshi, T. Murakami, T. Nagae, H. Noumi, H. Outa, K. Ozawa, T. Saito, J. Sasao, Y. Sato, S. Satoh, R. I. Sawafta, M. Sekimoto, T. Takahashi, L. Tang, H. H. Xia, S. H. Zhou, and L. H. Zhu, *Phys. Rev. Lett.* **86**, 1982 (2001).
- [3] O. Hashimoto and H. Tamura, *Prog. Part. Nucl. Phys.* **57**, 564 (2006).
- [4] D. J. Millener, A. Gal, C. Dover, and R. Dalitz, *Phys. Rev. C* **31**, 499 (1985).
- [5] Y. Yamamoto, T. Motoba, H. Himeno, K. Ikeda, and S. Nagata, *Prog. Theor. Phys. Suppl.* **117**, 361 (1994).
- [6] D. J. Millener, *Nucl. Phys. A* **691**, 93c (2001).
- [7] T. A. Rijken and Y. Yamamoto, *Phys. Rev. C* **73**, 044008 (2006).
- [8] Y. Fujiwara, Y. Suzuki, and C. Nakamoto, *Prog. Part. Nucl. Phys.* **58**, 439 (2007).
- [9] D. J. Millener, *Nucl. Phys. A* **804**, 84 (2008).
- [10] E. Hiyama and T. Yamada, *Prog. Part. Nucl. Phys.* **63**, 339 (2009).
- [11] R. H. Dalitz and A. Gal, *Phys. Rev. Lett.* **36**, 362 (1976).
- [12] T. Motoba, H. Bandō, K. Ikeda, and T. Yamada, *Prog. Theor. Phys. Suppl.* **81**, 42 (1985).
- [13] T. Motoba, H. Bandō, and K. Ikeda, *Prog. Theor. Phys.* **70**, 189 (1983).
- [14] H. Bandō, *Nucl. Phys. A* **450**, 217c (1986).
- [15] K. Itonaga, T. Motoba, O. Richter, and M. Sotona, *Phys. Rev. C* **49**, 1045 (1994).
- [16] E. Hiyama, M. Kamimura, K. Miyazaki, and T. Motoba, *Phys. Rev. C* **59**, 2351 (1999).
- [17] X.-R. Zhou, H.-J. Schulze, H. Sagawa, C.-X. Wu, and E.-G. Zhao, *Phys. Rev. C* **76**, 034312 (2007).
- [18] M. T. Win and K. Hagino, *Phys. Rev. C* **78**, 054311 (2008).
- [19] H.-J. Schulze, M. T. Win, K. Hagino, and H. Sagawa, *Prog. Theor. Phys.* **123**, 569 (2010).
- [20] M. Isaka, M. Kimura, A. Doté, and A. Ohnishi, *Phys. Rev. C* **83**, 044323 (2011).
- [21] P. H. Pile, S. Bart, R. E. Chrien, D. J. Millener, R. J. Sutter, N. Tsoupas, J.-C. Peng, C. S. Mishra, E. V. Hungerford, T. Kishimoto, L.-G. Tang, W. von Witsch, Z. Xu, K. Maeda, D. Gill, R. McCrady, B. Quinn, J. Seydoux, J. W. Sleight, R. L. Stearns, H. Plendl,

- A. Rafatian, and J. Reidy, *Phys. Rev. Lett.* **66**, 2585 (1991).
- [22] S. Ajimura, K. Aoki, H. Bhang, T. Endo, Y. Fujii, O. Hashimoto, H. Hotchi, E. Hungerford, J. Kim, Y. Kim *et al.*, *Nucl. Phys. A* **639**, 93c (1998).
- [23] B.-N. Lu, E.-G. Zhao, and S.-G. Zhou, *Phys. Rev. C* **84**, 014328 (2011).
- [24] T. Yamada, K. Ikeda, H. Bandō, and T. Motoba, *Prog. Theor. Phys.* **71**, 985 (1984).
- [25] M. Isaka, M. Kimura, A. Doté, and A. Ohnishi, *Phys. Rev. C* **83**, 054304 (2011).
- [26] D. Kurath, *Phys. Rev. C* **5**, 768 (1972).
- [27] A. Hayashi, K. Hara, and P. Ring, *Phys. Rev. Lett.* **53**, 337 (1984).
- [28] P. Bonche, H. Flocard, P. H. Heenen, S. J. Krieger, and M. S. Weiss, *Nucl. Phys. A* **443**, 39 (1985).
- [29] N. Redon, J. Meyer, M. Meyer, P. Quentin, M. S. Weiss, P. Bonche, H. Flocard, and P. H. Heenen, *Phys. Lett. B* **181**, 223 (1986).
- [30] M. Girod, J.-P. Delaroche, A. Gorgen, and A. Obertelli, *Phys. Lett. B* **676**, 39 (2009).
- [31] Z. P. Li, T. Nikšić, D. Vretenar, and J. Meng, *Phys. Rev. C* **81**, 034316 (2010).
- [32] J. A. Sheikh, Y. Sun, and R. Palit, *Phys. Lett. B* **507**, 115 (2011).
- [33] M. T. Win, K. Hagino, and T. Koike, *Phys. Rev. C* **83**, 014301 (2011).
- [34] J. M. Yao, Z. P. Li, K. Hagino, M. T. Win, Y. Zhang, and J. Meng, [arXiv:1104.3200v1](https://arxiv.org/abs/1104.3200v1).
- [35] R. Batchelor, A. Ferguson, H. Gove, and A. Litherland, *Nucl. Phys.* **16**, 38 (1960).
- [36] A. Cohen and J. Cookson, *Nucl. Phys.* **29**, 604 (1962).
- [37] M. Girod and B. Grammaticos, *Phys. Rev. C* **27**, 2317 (1983).
- [38] M. Bender and P.-H. Heenen, *Phys. Rev. C* **78**, 024309 (2008).
- [39] T. R. Rodríguez and J. L. Egido, *Phys. Rev. C* **81**, 064323 (2010).
- [40] M. Kimura, R. Yoshida, and M. Isaka, *Prog. Theor. Phys.* **127**, 287 (2012).
- [41] J. Decharge and D. Gogny, *Phys. Rev. C* **21**, 1568 (1980).
- [42] D. E. Lanskoj and Y. Yamamoto, *Phys. Rev. C* **55**, 2330 (1997).
- [43] T. Suhara and Y. Kanada-En'yo, *Prog. Theor. Phys.* **123**, 303 (2010).
- [44] P. M. Endt, *Nucl. Phys. A* **521**, 1 (1990).